Inorganic Chemistry

Article

pubs.acs.org/IC

Tunable Blue-Green-Emitting $Ba_3LaNa(PO_4)_3F:Eu^{2+},Tb^{3+}$ Phosphor with Energy Transfer for Near-UV White LEDs

Mengmeng Jiao,[†,‡] Ning Guo,[†,‡] Wei Lü,[†] Yongchao Jia,[†,‡] Wenzhen Lv,[†,‡] Qi Zhao,[†,‡] Baiqi Shao,[†,‡] and Hongpeng You*[,†]

[†]State Key Laboratory of Rare Earth Resource Utilization, Changchun Institute of Applied Chemistry, Chinese Academy of Science, Changchun 130022, P. R. China

[‡]University of the Chinese Academy of Science, Beijing 100049, P. R. China

Supporting Information

ABSTRACT: A series of Eu^{2+} and Eu^{2+}/Tb^{3+} activated novel $Ba_3LaNa(PO_4)_3F$ phosphors have been synthesized by traditional solid state reaction. Rietveld structure refinement of the obtained phosphor indicates that the $Ba_3LaNa(PO_4)_3F$ host contains three kinds of Ba sites. The photoluminescence properties exhibit that the obtained phosphors can be efficiently excited in the range from 320 to 430 nm, which matches perfectly with the commercial n-UV LED chips. The critical distance of the Eu^{2+} ions in $Ba_3LaNa(PO_4)_3F:Eu^{2+}$ is calculated and the energy quenching mechanism is proven to be dipole−dipole interaction. Tunable blue-green emitting $Ba_3LaNa(PO_4)_3F:Eu^{2+},Tb^{3+}$ phosphor has been obtained by co-doping Eu^{2+} and Tb^{3+} ions into the host and varying their relative ratios. Compared with the Tb^{3+} singly doped phosphor, the codoped phosphors have more intense absorption in the n-UV range and stronger emission of the Tb^{3+} ions, which are attributed to the effective energy transfer from the Eu^{2+} to Tb^{3+} ions. The energy transfer from the Eu^{2+} to Tb^{3+} ions is demonstrated to be a dipole−quadrupole mechanism by the Inokuti-Hirayama (I−H) model. The Eu^{2+} and Tb^{3+} activated phosphor may be good candidates for blue-green components in n-UV white LEDs.

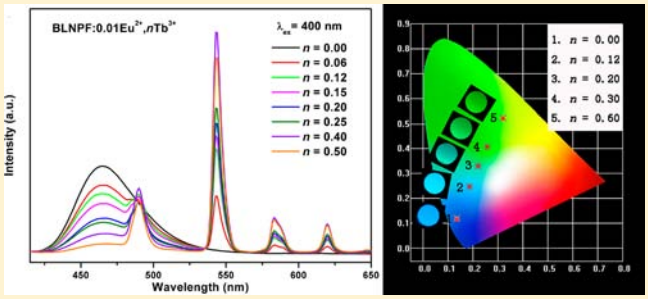

INTRODUCTION

White light emitting diodes had been regarded as the next generation lighting source due to their merits of long lifetime, environmental friendliness, and high efficiency, compared with conventional incandescent and fluorescence lamps.[1−5] The main strategy to obtain WLEDs is the combination of blue or near-ultraviolet (n-UV) LEDs with one or more phosphors, known as phosphor converted-LEDs (pc-LEDs). At present, the combination of $Y_3Al_5O_{12}:Ce^{3+}$ (YAG:Ce) phosphor with blue InGaN chip is most frequently used.[6,7] However, this method suffers the problems of low color rendering index (Ra < 80) and high correlated color temperature (Tc > 4500 K), restricting their application.[8,9] Another approach to obtain white light is the combination of n-UV (380−420 nm) LED chips with tricolor (red, green, and blue) phosphors. WLEDs fabricated in this way can overcome the above problems and produce an excellent color rendering index and easily controlled emission color properties.[10−12] In this case, it is essential to find novel phosphors that can be efficiently excited by the n-UV LED chips.

The Eu^{2+} ion is one of the most common activators for phosphors due to the intense and broad excitation and emission bands derived from their dipole allowed 4f−5d electronic transitions. The emission wavelength of the Eu^{2+} ions can vary from n-UV to red region depending on different hosts. Strong ligand−activator bonding interactions will cause low energy difference between the $4f^65d^1$ and $4f^7$ states, and thus, leading to a red shift of the emission band of the Eu^{2+} ions.[13−16] Moreover, for Eu^{2+} ions, the Stokes shift is relatively small and the decay time is short, making the Eu^{2+} a popular activator. In recent years, the photoluminescence properties of the Eu^{2+} ions in many hosts had been studied, such as $Li_2SrSiO_4:Eu^{2+}$,[17] $Ca_2Al_3O_6F:Eu^{2+}$,[18] and $Sr_8MgLn(PO_4)_7:Eu^{2+}$.[19] The Tb^{3+} ion is regarded as a promising green-emitting activator for showing sharp lines at about 488, 543, and 582 nm due to the 4f−4f transition. The major problem for the Tb^{3+} ion is the lack of efficient and broad excitation band from n-UV region to visible range, which limits its application in n-UV white LEDs. Moreover, since the f−f transition is spin-forbidden, the emission intensity of the Tb^{3+} ion is weak. An efficacious way to solve the above problem is by utilizing energy transfer from sensitizers to activators in a proper host.[20−22] Since the Eu^{2+} ion may be a good sensitizer for the Tb^{3+} ion, it is important to study the luminescence properties of the Eu^{2+} and Tb^{3+} co-doped phosphors.[23]

Phosphors based on fluorophosphates have attracted great interest in recent years since they show good chemical and thermal stability. Moreover, the fluorine atoms have the largest electronegative and exhibit strongest attractive electron ability

Received: April 25, 2013
Published: August 30, 2013

   dx.doi.org/10.1021/ic401033u | Inorg. Chem. 2013, 52, 10340−10346

and phosphors which contain the fluorine atoms usually have good luminescence properties. For example, Huang et al. reported the $Ca_2RF_4PO_4:Eu^{3+}$ (R = Gd, Y) as a potential red-emitting phosphor.[24] Geng et al. described the luminescence properties of $Ca_2YF_4PO_4:Eu^{2+},Mn^{2+}$ phosphor[25] and Zhang et al. reported the $Ca_5(PO_4)_3F:Ce^{3+},Mn^{2+}$ as a single-component phosphor for WLEDs.[26] However, the report on the $Ba_3LaNa(PO_4)_3F$ phosphors is lack. Herein we report structure and luminescence properties of Eu^{2+}/Tb^{3+} activated $Ba_3LaNa(PO_4)_3F$ phosphors. The obtained samples have intense broad excitation bands ranging from 320 to 430 nm which matches well with the popular n-UV LED chips. At the excitation of 400 nm, the $Ba_3LaNa(PO_4)_3F:Eu^{2+}$ can exhibit a blue emission band which extends from 425 to 525 nm. In Eu^{2+} and Tb^{3+} codoped phosphor, a series of tunable blue-greenish colors can be obtained by varying the relative ratio of Eu^{2+}/Tb^{3+} in the irradiation of 400 nm. By utilizing the energy transfer between the Eu^{2+} and Tb^{3+} ions, we get intense blue-green phosphor which can be efficiently excited by n-UV LEDs. Moreover, the energy transfer mechanism between the Eu^{2+} and Tb^{3+} ions has been investigated systematically.

EXPERIMENTAL SECTION

Materials and Synthesis. A series of $(Ba_{1-m}Eu_m)_3La_{1-n}Tb_nNa(PO_4)_3F$ (BLNPF:mEu^{2+},nTb^{3+}, m = 0−0.07, n = 0−0.60) phosphors were synthesized by conventional high temperature solid-state reaction. The starting materials $BaCO_3$ (A.R.), BaF_2 (A.R.), La_2O_3 (A.R.), Na_2CO_3 (A.R.), $NH_4H_2PO_4$ (A.R.), Eu_2O_3 (99.99%), and Tb_4O_7 (99.99%) were weighed in a proper stoichiometric ratio with 10% excess of BaF_2 for the loss of fluorine. After mixing and grinding in an agate mortar for 15 min, the mixture was placed in a crucible and then sintered at 1050 °C for 3 h in a reductive atmosphere (20% H_2 + 80% N_2). Finally, the prepared phosphors were cooled to room temperature and reground for further measurements.

Measurements and Characterization. The powder X-ray diffraction (XRD) measurements were performed on D8 Focus diffractometer (Bruker) operating at 40 kV and 40 mA with Cu Kα radiation (λ = 1.5418 Å). The scanning rate was fixed at 10°/ min with 2θ ranges from 15° to 80°. The photoluminescence (PL) and photoluminescence excitation (PLE) spectra were measured by a Hitachi F-4500 spectrophotometer equipped with a 150 W xenon lamp as the excitation source. In fluorescence lifetime measurements, a tunable laser (pulse width = 4 ns, gate = 50 nm) was used as an excitation source, and the signals were detected with a Lecroy Wave Runner 6100 digital oscilloscope (1 GHz). The above measurements were performed at room temperature. The spectra at 4.3 and 298.0 K were performed on the Edinburgh Instrument FLS 920 spectrophotometer with the advanced research system InC as the temperature controlling system.

RESULTS AND DISCUSSION

Phase Identification and Crystal Structure. All the prepared samples were characterized by the powder X-ray diffraction to verify their phase purity. Figure 1 demonstrates the typical powder XRD patterns of BLNPF:0.01Eu^{2+}, BLNPF:0.03Eu^{2+}, and BLNPF:0.01Eu^{2+},0.50Tb^{3+} samples. It is obvious that all the diffraction peaks can be indexed to the standard data of $Ba_3LaNa(PO_4)_3F$ (JCPDS 71−1317) indicating that our prepared samples are of phase purity and the doped ions do not cause any significant change. Considering the ionic radii and valence state of Eu^{2+}/Ba^{2+} and Tb^{3+}/La^{3+} ions,[27] we suppose that the Eu^{2+} and Tb^{3+} ions occupy the Ba^{2+} and La^{3+} sites, respectively. From Figure 1 one can also see that the diffraction peaks of the phosphors shift to a higher angle with the doping of rare earth ions. This phenomenon is

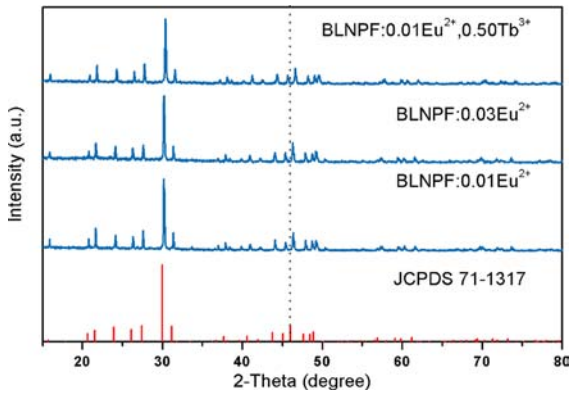

Figure 1. XRD patterns of typical prepared samples and standard data for $Ba_3LaNa(PO_4)_3F$ (JCPDS card no.71−1317).

associated with the substituting of larger Ba^{2+} and La^{3+} ions by smaller Eu^{2+} and Tb^{3+} ions and can reflect that the doped ions are completely incorporated into the host.

To further study the structure of the obtained samples, Rietveld structure refinement of $(Ba_{0.98}Eu_{0.02})_3LaNa(PO_4)_3F$ phosphor was performed using the general structure analysis system (GSAS) program.[28] Figure 2a depicts the results of Rietveld refinement pattern of the Eu^{2+} doped sample. In the refinement, the previously reported crystallographic data of $Ba_3LaNa(PO_4)_3F$ (ICSD#010030) which crystallizes in a hexagonal unit cell with the space group $P\bar{6}$ (174) was

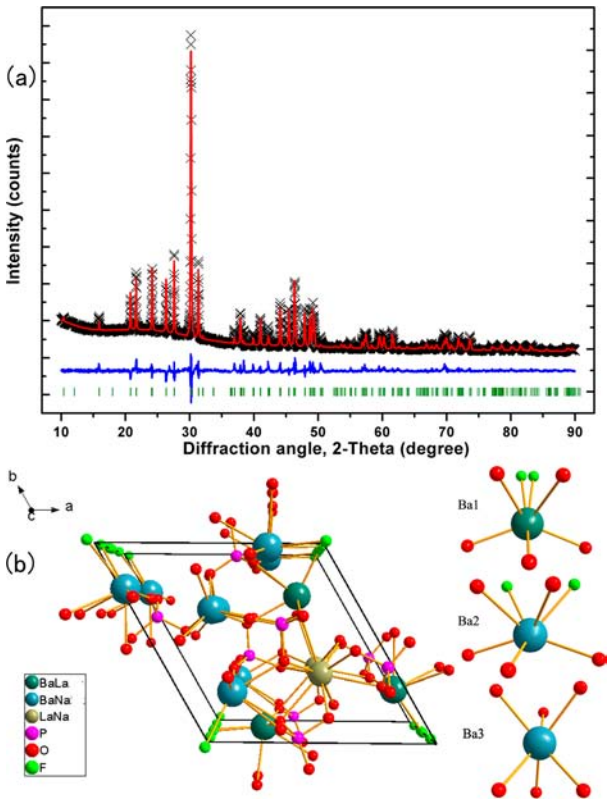

Figure 2. (a) Experimental (crosses) and calculated (red solid line) powder XRD pattern of the BLNPF:0.02Eu^{2+} sample. The blue solid lines represent the difference between experimental and calculated data and the red sticks mark the Bragg reflection positions. (b) Unit cell structure of $Ba_3LaNa(PO_4)_3F$ and coordination environment of the Ba^{2+} ions.

dx.doi.org/10.1021/ic401033u | Inorg. Chem. 2013, 52, 10340−10346

employed as initial structure model. The final refinement structure parameters are listed in Table S1 (Supporting Information). The refinement data χ^2 = 6.077, R_{wp} = 7.81%, and R_p = 5.63% indicate that all atom positions, fraction factors, and temperature factors satisfy the reflection condition. For $(Ba_{0.98}Eu_{0.02})_3LaNa(PO_4)_3F$ sample, the cell parameters were determined to be $a = b$ = 9.898411 Å, c = 7.386219 Å, and V = 626.735 Å^3. Figure 2b shows the unit cell structure of BLNPF:0.02Eu^{2+} sample together with the coordination environments of the Ba^{2+} sites. In $Ba_3LaNa(PO_4)_3F$ host, there are three kinds of Ba^{2+} sites which are named Ba1, Ba2, and Ba3 here for easier identification.[29] The Ba1 and Ba2 sites are seven coordinated with five oxygen atoms and two fluorine atoms, while the Ba3 site is coordinated with six oxygen atoms. From the refinement results, the average length of different Ba−O and Ba−F bonds were calculated and shown as follows: Ba1−O is 2.6832 Å, Ba1−F is 2.4360 Å; Ba2−O is 2.7485 Å, Ba2−F is 2.8259 Å; Ba3−O is 2.5498 Å. The cations in the host are connected by the $[PO_4]^{3-}$ tetrahedral formed by the P and O atoms.

Luminescence Properties of Eu^{2+}-Doped Materials. Figure 3 depicts the photoluminescence (PL) and photo-

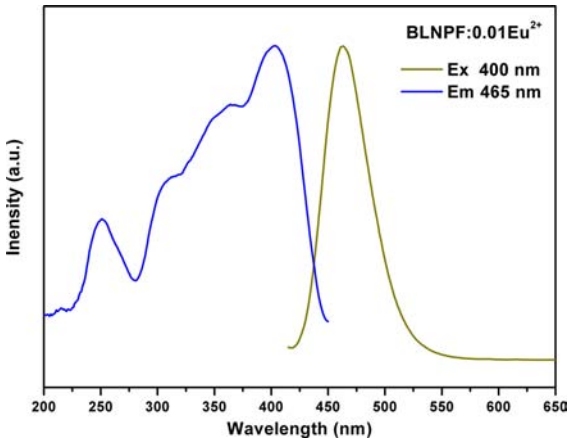

Figure 3. PL and PLE spectra of BLNPF:0.01Eu^{2+} phosphor.

luminescence excitation (PLE) spectra of the as-prepared BLNPF:0.01Eu^{3+} phosphor. Monitored at 465 nm, the sample shows a narrow weak excitation band from 230 to 280 nm and a broad intense band from 280 to 430 nm with a maxium at 400 nm due to the $4f^7 \rightarrow 4f^6 5d^1$ transition of the Eu^{2+} ions. The excitation spectrum indicates that the phosphor matches well with the commercial n-UV LED chips (360−410 nm).[30] At the excitation of 400 nm, the PL spectrum shows an intense blue emission band attributed to the $4f^6 5d^1 \rightarrow 4f^7$ transition of the Eu^{2+} ion. The emission spectra of the BLNPF:0.01Eu^{2+} phosphor at 4.3 and 298 K were measured and demonstrated in Figure 4. It can be seeen that the emission spectrum at 4.3 K with fwhm being 35 nm is much narrower than that at 298 K with fwhm being 48 nm. This difference should be associated with the vibration energy of the host lattice. The $4f^6 5d^1 \rightarrow 4f^7$ transition has strong coupling with the energy of the phonon vibrations in host and this vibronic coupling can lead to broadened emission band in the phosphor. At 4.3 K, the number of phonon vibrations are restricted and the emission band is narrow. With increasing temperature, the number of separate phonon branches increases and the emission band is broadened. From this figure one can also see that the emission

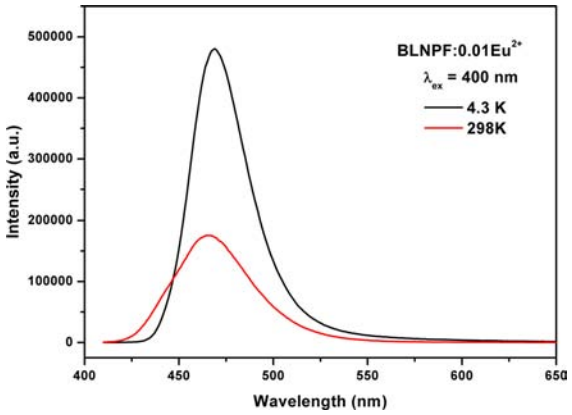

Figure 4. Emission spectra of BLNPF:0.01Eu^{2+} phosphor at 4.3 and 298 K.

spectra at 4.3 and 298.0 K are asymmetric, indicating that there are more than one Eu^{2+} emitting centers in the host.

In order to investigate the effect of doping concentration on luminescence properties, a series of BLNPF:mEu^{2+} (m = 0.005, 0.01, 0.02, 0.03, 0.04, 0.05, 0.06, 0.07) phosphors were synthesized. Figure 5 shows the PL spectra of BLNPF:mEu^{2+}

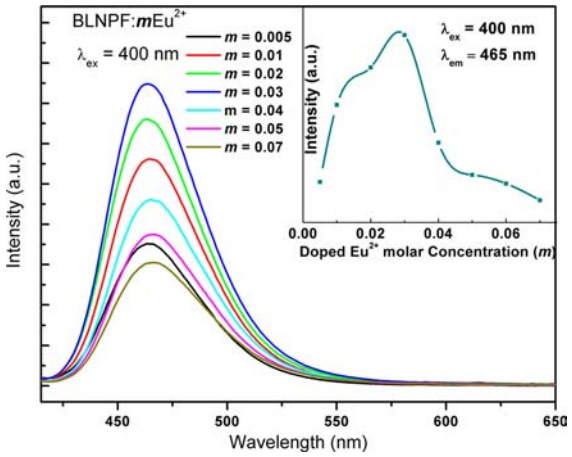

Figure 5. Emission spectra for BLNPF:mEu^{2+} with various doped Eu^{2+} molar concentration (m). (Inset shows the variation of emission intensity as a function of doped Eu^{2+} molar concentration).

with different doping contents. The blue emission of the Eu^{2+} increases gradually and reaches a maximum at m = 0.03. With further increment of Eu^{2+} concentration, the emission intensity begins to decrease due to concentration quenching. According to the Dexter's energy transfer theory,[31] concentration quenching is mainly caused by the nonradiative energy migration among the Eu^{2+} ions at the high concentration. The critical distance between the Eu^{2+} ions can be calculated using the following equation:[32]

$$R_C \approx 2\left[\frac{3V}{4\pi x_c N}\right]^{1/3} \quad (1)$$

where V is the volume of the unit cell, N represents the number of sites that the Eu^{2+} can occupy in per unit cell, and x_c is the critical concentration. For BLNPF host, V = 626.74 Å^3, N = 6, and x_c = 0.03, therefore, the critical distance R_C is calculated to be 18.80 Å. In oxide phosphor, nonradiative energy transfer usually occurs as a result of exchange interaction or multipole−

dx.doi.org/10.1021/ic401033u | Inorg. Chem. 2013, 52, 10340−10346

multipole interaction.[33] Since the exchange interaction comes into effect only when the distance between activators is shorter than 5 Å, the concentration quenching mechanism of the Eu^{2+} in the phosphor is dominated by the multipole−multipole interaction. According to Van Uiter's report, the emission intensity (I) per activator ion follows the equation[34]

$$I/m = k[1 + \beta(m)^{\theta/3}]^{-1} \quad (2)$$

where m is the activator concentration, I/m is the emission intensity per activator concentration, k and β are constants for a given host in the same excitation condition; and θ = 6, 8, and 10 represent the dipole−dipole, dipole−quadrupole, and quadrupole−quadrupole interactions, respectively. By modifying the eq 2, $\log(I/m)$ acts a liner function of $\log(m)$ with a slop of $(-\theta/3)$. To get the value of θ, the relationship between $\log(I/m)$ and $\log(m)$ is plotted with m ranging from 0.04 to 0.07. From Figure 6, the $\theta/3$ is determined to be 1.71, and

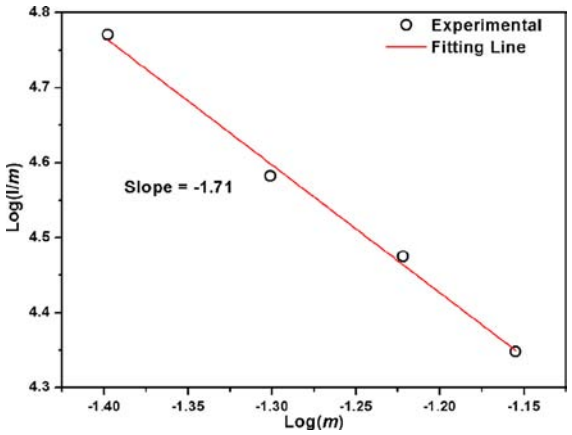

Figure 6. Dependence of $\log(I/m)$ on $\log(m)$ in BLNPF:$m$$Eu^{2+}$ phosphors.

accordingly, θ is calculated to be 5.13 which is close to 6. The result indicates that the concentration quenching mechanism of the Eu^{2+} emission in $Ba_3LaNa(PO_4)_3F$ host is dominated by the dipole−dipole interaction. For $Ba_3LaNa(PO_4)_3F$:Eu^{2+} phosphor, the CIE chromaticity coordinates were determined to be (0.133, 0.121), which located at the blue region of the CIE coordinate diagram. From the above photoluminescence study, we consider that the n-UV excited BLNPF:Eu^{2+} may have potential application as a blue phosphor for n-UV white LEDs.

Luminescence Properties of BLNPF:Eu^{2+},Tb^{3+} Phosphor and Energy Transfer Between the Eu^{2+} and Tb^{3+} Ions. Figure 7a illustrates the PL and PLE spectra of the BLNPF:0.10Tb^{3+} phosphor. The PLE spectrum monitored at 543 nm exhibits a broad band and several weak peaks. The broad band from 200 to 250 nm centered at 230 nm is ascribed to the f−d transitions of the Tb^{3+} ions, while the peaks in the wavelength ranging from 280 to 500 nm are due to the intra-$4f^8$ transitions. At the excitation of 230 nm, the as-prepared BLNPF:Tb^{3+} phosphor emits two sets of emissions. The emission peaks at 490, 543, 581, and 619 nm are assigned to the $^5D_4-^7F_J$ (J = 6,5,4,3) transitions, while the emission peaks at 380, 410, and 430 nm are due to the $^5D_3-^7F_J$ transitions. Since there is an overlap between the PL spectra of BLNPF:Eu^{2+} and PLE spectra of BLNPF:Tb^{3+} phosphors (Figure S1, Supporting Information), an effective energy transfer from the sensitizer Eu^{2+} to activator Tb^{3+} can be

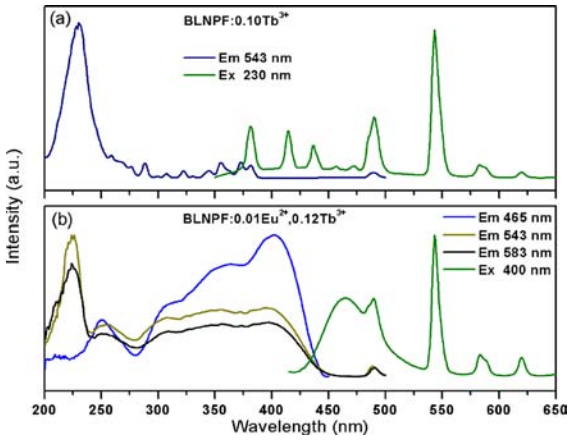

Figure 7. PL and PLE spectra of (a) BLNPF:0.10Tb^{3+} and (b) BLNPF:0.01Eu^{2+},0.12Tb^{3+} phosphors.

expected in the Eu^{2+} and Tb^{3+} codoped phosphor. Figure 7b shows the PLE and PL spectra of the BLNPF:0.01Eu^{2+}, 0.12Tb^{3+} phosphor. At the irradiation of 400 nm, the PL spectrum exhibits both the Eu^{2+} and the typical Tb^{3+} emissions. Monitored at 543 nm which is the typical emission of the Tb^{3+} ions due to its $^5D_4-^7F_5$ transition, the phosphor shows absorption of both the Tb^{3+} and Eu^{2+} ions comparing with the PLE spectrum monitored at 465 nm. To avoid the existence of the Eu^{2+} emission at 543 nm, we chose another emission peak at 583 nm ($^5D_4-^7F_5$ transition of the Tb^{3+} ion) as monitoring wavelength which is beyond the emission range of the Eu^{2+} ions. From Figure 7b, we can see that the PLE spectrum is similar to that monitored at 543 nm. The above analysis on the PLE and PL spectra of the BLNPF:0.01Eu^{2+}, 0.12Tb^{3+} phosphor proves the occurrence of the energy transfer from the Eu^{2+} to Tb^{3+} ions.

A series of phosphors with fixed Eu^{2+} or Tb^{3+} content were prepared to study the effect of doping concentration on the luminescence properties of phosphors. Figure 8a shows the PL spectra of the BLNPF:0.01Eu^{2+}, $n$$Tb^{3+}$ phosphors with n varying from 0 to 0.50. With an increasing of the Tb^{3+} content, the emission intensity of the Eu^{2+} decreases monotonically. However, the intensity of the Tb^{3+} emission first increases to a maximum at n = 0.40, then decreases due to the concentration quenching. In addition, Figure 8b depicts the PL spectra of the BLNPF:$m$$Eu^{2+}$,0.10$Tb^{3+}$ (m = 0.00−0.06) phosphors. For the Tb^{3+} single-doped sample, we could not see the emission of Tb^{3+} ion since it has no absorption at 400 nm. Although the content of the Tb^{3+} is fixed, the emission of Tb^{3+} dramatically increased with the doping of Eu^{2+} ions at a certain range, further confirming an efficient energy transfer from the Eu^{2+} to Tb^{3+} ions. As m varies from 0.01 to 0.06, the emission intensity of the Tb^{3+} first increased to a maximum at m = 0.03 and then decreased with further increment of Eu^{2+} content.

To further study the energy transfer process, the fluorescence decay curves of the Eu^{2+} ions in BLNPF:0.01Eu^{2+},$n$$Tb^{3+}$ phosphors were measured by monitoring at 465 nm with an irradiation of 355 nm. From Figure 9, one can see that all the decay curves deviate from the single exponential rule. With the incensement of the Tb^{3+} ions, this deviation becomes more obvious. The average fluorescence lifetimes of the Eu^{2+} ions in phosphors with different doping concentration of the Tb^{3+} are calculated by using the following equation:

dx.doi.org/10.1021/ic401033u | Inorg. Chem. 2013, 52, 10340−10346

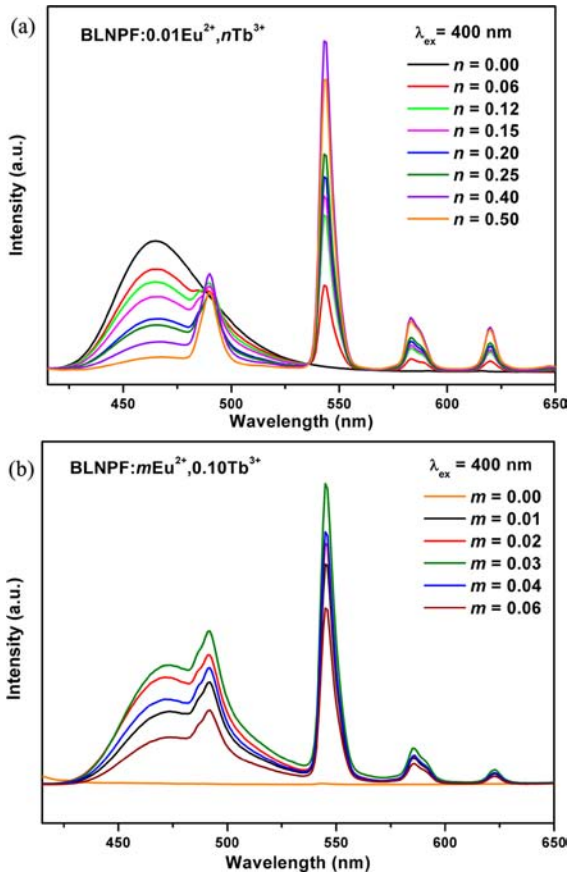

Figure 8. PL spectra of BLNPF:Eu^{2+},Tb^{3+} phosphors with various (a) Tb^{3+} content and (b) Eu^{2+} content.

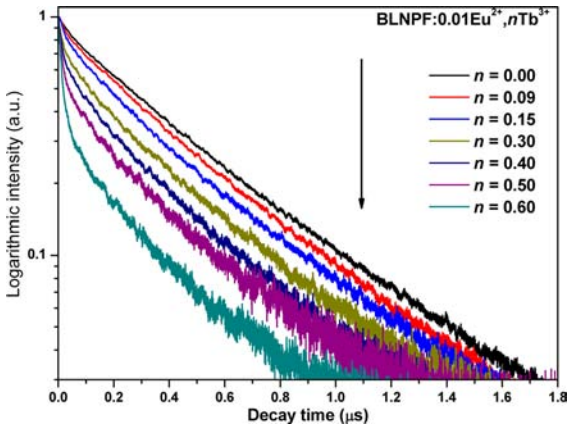

Figure 9. Decay curves for the luminescence of Eu^{2+} ions in BLNPF:0.01Eu^{2+},nTb^{3+} samples. (excited at 355 nm, monitored at 465 nm).

$$\tau_{avg} = \int_0^\infty I(t)t\ dt / \int_0^\infty I(t)\ dt \tag{3}$$

where the $I(t)$ represents the luminescence intensity at time t. On the basis of eq 3, the lifetimes of the Eu^{2+} ions are determined to be 0.40, 0.39, 0.35, 0.33, 0.31, 0.26, 0.24, and 0.21 μs for the BLNPF:0.01Eu^{2+},nTb^{3+} phosphors with n = 0.06, 0.12, 0.20, 0.25, 0.30, 0.40, 0.50, and 0.60, respectively. Energy transfer efficiency η_T between the Eu^{2+} and Tb^{3+} ions was also obtained from the decay lifetime by using the equation[35]

$$\eta_T = 1 - \frac{\tau}{\tau_0} \tag{4}$$

where the τ and τ_0 are the lifetimes of sensitizer (Eu^{2+}) ion with and without the presence of activator (Tb^{3+}), respectively. The lifetimes and energy transfer efficiencies are plotted as a function of the Tb^{3+} concentration and shown in Figure 10.

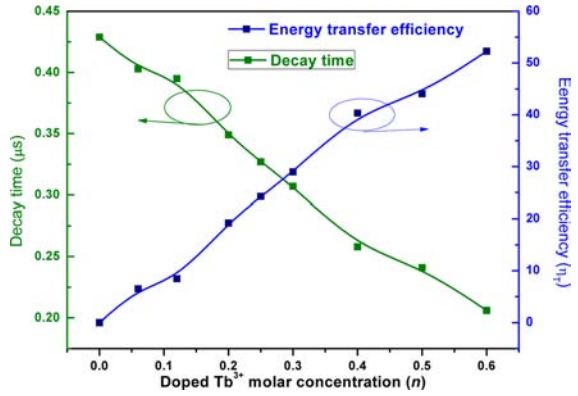

Figure 10. Dependence of the fluorescence lifetime of the Eu^{2+} and energy transfer efficiency on doped Tb^{3+} molar concentration in BLNPF:0.01Eu^{2+},nTb^{3+} samples.

From that one can see the average lifetimes decrease monotonously while the energy transfer efficiency increases gradually with the increment of the Tb^{3+} ions. The value of η_T reaches the maximum of 52.3% when n = 0.60, indicating that the energy transfer from the Eu^{2+} to Tb^{3+} is efficient.

To analyze the energy transfer mechanism, we employed the Inokuti-Hirayama (I–H) model[36] which can be used when the energy migration process can be negligible compared to the energy transfer between donors and acceptors. The normalized intensity of the donor fluorescence can be written as

$$I_D(t) = I_{D0}(t)f(t) \tag{5}$$

where $I_{D0}(t)$ is the decay function of donors without the acceptors, the function $f(t)$ characterizes the loss of excited donors due to one-way energy transfer to the acceptors. If the energy transfer rate between a donor and an acceptor is inversely proportional to the distance, according to the I–H formula,[36] we can get

$$f(t) = \exp\left[-\frac{4}{3}\pi\Gamma\left(1 - \frac{3}{m}\right)n_A\alpha^{3/m}t^{3/m}\right] \tag{6}$$

where n_A is the number of acceptor ions per unit volume, α is the rate constant for energy transfer, the coefficient m = 6, 8, and 10 corresponds for dipole–dipole, dipole–quadrupole, and quadrupole–quadrupole interactions, respectively. By modifying eqs 5 and 6, we obtained

$$\log\{\ln[I_{D0}(t)/I_D(t)]\} \propto \frac{3}{m}\log(t) \tag{7}$$

From the above result, we can see that $\log\{\ln[I_{D0}(t)/I_D(t)]\}$ acts as a linear function of $\log(t)$ with a slope of $3/m$. To obtain a correct m value in this case, we plotted the $\log\{\ln[I_{D0}(t)/I_D(t)]\}$ as a function of $\log(t)$ for the prepared BLNPF:0.01Eu^{2+},nTb^{3+} phosphors, and the fitting results are shown in Figure 11. From the calculated slope of the fitting lines, the values of m are estimated to be 7.87, 8.33, and 8.04 for BLNPF:0.01Eu^{2+},nTb^{3+} samples with n = 0.06, 0.15, and 0.30,

dx.doi.org/10.1021/ic401033u | Inorg. Chem. 2013, 52, 10340–10346

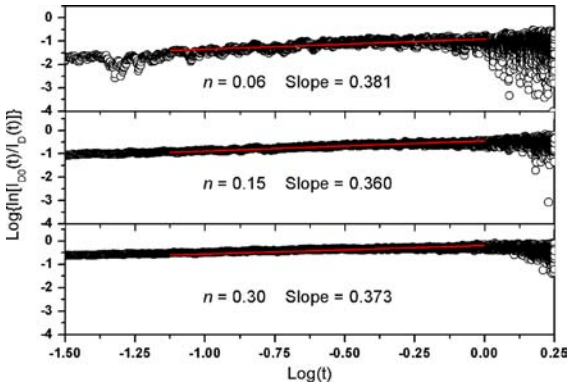

Figure 11. Experimental data plots of $\log\{\ln[I_{D0}(t)/I_D(t)]\}$ versus $\log(t)$ of Eu^{2+} in BLNPF:0.01Eu^{2+},nTb^{3+} (n = 0.06, 0.15, 0.30) samples. The red lines indicate the fitting behaviors.

respectively. Since the calculated values of m are nearly consistent with 8, the energy transfer from the Eu^{2+} to Tb^{3+} ions in BLNPF host is thought to be dominated by dipole−quadrupole mechanism.

Figure 12 shows the Commission International de L'Eclairage (CIE) chromaticity diagram for several typical

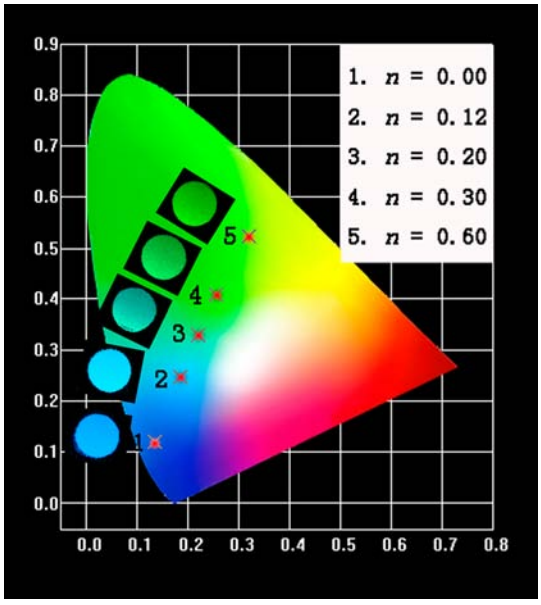

Figure 12. CIE chromaticity diagram for BLNPF:0.01Eu^{2+},nTb^{3+} phosphors, together with their corresponding photographs under a 365 nm UV lamp.

BLNPF:0.01Eu^{2+},nTb^{3+} samples, together with their corresponding photographs. It can be seen that the emitting color of the phosphors can be easily modulated from blue to green by simply varying the value of n from 0 to 0.60. Accordingly, the corresponding CIE coordinates of BLNPF:0.01Eu^{2+},nTb^{3+} change from (0.133, 0.121) to (0.319, 0.523), due to the different emission composition of the Eu^{2+} and Tb^{3+} ions. Thus, blue-green emitting phosphors which can be efficiently excited by the n-UV chips are obtained via the energy transfer from the Eu^{2+} to Tb^{3+} ions and the BLNPF:Eu^{2+},Tb^{3+} phosphor may have potential value as blue-greenish phosphors used for n-UV white LEDs.

CONCLUSIONS

In summary, a series of Eu^{2+}/Tb^{3+} activated $Ba_3LaNa(PO_4)_3F$ phosphors had been synthesized and investigated for the first time. The $Ba_3LaNa(PO_4)_3F$ host has a hexagonal unit cell with cell parameters $a = b = 9.898411$ Å, $c = 7.386219$ Å, and $V = 626.735$ Å^3, and $Z = 2$. The obtained phosphors have a broad excitation band ranging from 320 to 430 nm which can match perfectly with the commercial n-UV LED chips. At the excitation of 400 nm, the $Ba_3LaNa(PO_4)_3F:Eu^{2+}$ phosphors can emit intense blue light with an optimal concentration of the Eu^{2+} being 0.03. The critical distance for the Eu^{2+} has also been calculated to be 18.80 Å and the concentration quenching is dominated by dipole−dipole interaction. For the co-doped samples, tunable colors from blue to green can be realized by singly varying the doping concentration of the Tb^{3+} ion at the irradiation of 400 nm. The dipole−quadrupole interaction mechanism should be mainly responsible for the energy transfer from the Eu^{2+} to Tb^{3+} ions. The experimental results indicate that the $Ba_3LaNa(PO_4)_3F:Eu^{2+},Tb^{3+}$ phosphor may have promising application in n-UV white LEDs.

ASSOCIATED CONTENT

Supporting Information

Final refined structure parameters of BLNPF:0.02Eu^{2+} and PL spectral overlap. This material is available free of charge via the Internet at http://pubs.acs.org.

AUTHOR INFORMATION

Corresponding Author

*E-mail: hpyou@ciac.jl.cn.

Notes

The authors declare no competing financial interest.

ACKNOWLEDGMENTS

This work is financially supported by the National Natural Science Foundation of China (Grant No. 21271167) and the Fund for Creative Research Groups (Grant No. 21221061).

REFERENCES

(1) Brinkley, S. E.; Pfaff, N.; Denault, K. A.; Zhang, Z.; Hintzen, H. B.; Seshadri, R.; Nakamura, S.; DenBaars, S. P. *Appl. Phys. Lett.* **2011**, *99*, 241106.
(2) Krings, M.; Montana, G.; Dronskowski, R.; Wickleder, C. *Chem. Mater.* **2011**, *23*, 1694−1699.
(3) Lin, C. C.; Liu, R.-S. *J. Phys. Chem. Lett.* **2011**, *2*, 1268−1277.
(4) Suehiro, T.; Hirosaki, N.; Xie, R.-J. *ACS Appl. Mater. Interfaces* **2011**, *3*, 811−816.
(5) Won, Y.-H.; Jang, H. S.; Jeon, D. Y. *J. Electrochem. Soc.* **2011**, *158*, J276−J281.
(6) Bachmann, V.; Ronda, C.; Meijerink, A. *Chem. Mater.* **2009**, *21*, 2077−2084.
(7) Jia, Y.; Huang, Y.; Zheng, Y.; Guo, N.; Qiao, H.; Zhao, Q.; Lv, W.; You, H. P. *J. Mater. Chem.* **2012**, *22*, 15146−15152.
(8) Hao, Z.; Zhang, J.; Zhang, X.; Sun, X.; Luo, Y.; Lu, S.; Wang, X.-j. *Appl. Phys. Lett.* **2007**, *90*, 261113.
(9) Shi, Y.; Wang, Y.; Wen, Y.; Zhao, Z.; Liu, B.; Yang, Z. *Opt. Express* **2012**, *20*, 21656−21664.
(10) Im, W. B.; Brinkley, S.; Hu, J.; Mikhailovsky, A.; DenBaars, S. P.; Seshadri, R. *Chem. Mater.* **2010**, *22*, 2842−2849.
(11) Jung, K. Y.; Lee, H. W.; Jung, H.-K. *Chem. Mater.* **2006**, *18*, 2249−2255.
(12) Zhang, S.; Nakai, Y.; Tsuboi, T.; Huang, Y.; Seo, H. J. *Inorg. Chem.* **2011**, *50*, 2897−2904.

(13) Hecht, C.; Stadler, F.; Schmidt, P. J.; auf der Günne, J. r. S.; Baumann, V.; Schnick, W. *Chem. Mater.* **2009**, *21*, 1595−1601.
(14) Hou, D.; Liu, C.; Ding, X.; Kuang, X.; Liang, H.; Sun, S.; Huang, Y.; Tao, Y. *J. Mater. Chem. C* **2013**, *1*, 493−499.
(15) Lizzo, S.; Velders, A. H.; Meijerink, A.; Dirksen, G. J.; Blasse, G. *J. Lumin.* **1995**, *65*, 303−311.
(16) Lü, W.; Hao, Z.; Zhang, X.; Luo, Y.; Wang, X.; Zhang, J. *Inorg. Chem.* **2011**, *50*, 7846−7851.
(17) Saradhi, M. P.; Varadaraju, U. *Chem. Mater.* **2006**, *18*, 5267−5272.
(18) Xia, Z.; Liu, R.-S.; Huang, K.-W.; Drozd, V. *J. Mater. Chem.* **2012**, *22*, 15183−15189.
(19) Huang, C.-H.; Chen, T.-M. *Inorg. Chem.* **2011**, *50*, 5725−5730.
(20) Guo, N.; Song, Y.; You, H.; Jia, G.; Yang, M.; Liu, K.; Zheng, Y.; Huang, Y.; Zhang, H. *Eur. J. Inorg. Chem.* **2010**, *2010*, 4636−4642.
(21) Jia, D.; Meltzer, R.; Yen, W.; Jia, W.; Wang, X. *Appl. Phys. Lett.* **2002**, *80*, 1535−1537.
(22) You, H.; Wu, X.; Hong, G.; Tang, J.; Hu, H. *Chem. Mater.* **2003**, *15*, 2000−2004.
(23) Lee, B. H.; Jeong, H. G.; Sohn, K.-S. *J. Electrochem. Soc.* **2010**, *157*, J227−J232.
(24) Huang, Y.; Nakai, Y.; Tsuboi, T.; Seo, H. J. *Opt. Express* **2011**, *19*, 6003−6011.
(25) Geng, D.; Shang, M.; Zhang, Y.; Cheng, Z.; Lin, J. *Eur. J. Inorg. Chem.* **2013**, *16*, 2947−2953.
(26) Zhang, C.; Huang, S.; Yang, D.; Kang, X.; Shang, M.; Peng, C.; Lin, J. *J. Mater. Chem.* **2010**, *20*, 6674−6680.
(27) Shannon, R. D. *Acta Crystallogr., Sect. A: Cryst. Phys., Diffr., Theor. Gen. Crystallogr.* **1976**, *32*, 751.
(28) Larson, A. C.; Von Dreele, R. B. *Los Alamos Natl. Lab. [Rep.] LAUR.* **1994**, *86*, 748.
(29) Mathew, M.; Mayer, I.; Dickens, B.; Schroeder, L. *J. Solid State Chem.* **1979**, *28*, 79−95.
(30) Jia, Y.; Lü, W.; Guo, N.; zhen Lv, W.; Zhao, Q.; You, H. *Chem. Commun.* **2013**, *49*, 2664−2666.
(31) Dexter, D.; Schulman, J. H. *J. Chem. Phys.* **1954**, *22*, 1063−1070.
(32) Blasse, G. *Philips Res. Rep.* **1969**, *24*, 131.
(33) Dexter, D. L. *J. Chem. Phys.* **1953**, *21*, 836−850.
(34) Guo, N.; You, H.; Song, Y.; Yang, M.; Liu, K.; Zheng, Y.; Huang, Y.; Zhang, H. *J. Mater. Chem.* **2010**, *20*, 9061−9067.
(35) Paulose, P.; Jose, G.; Thomas, V.; Unnikrishnan, N.; Warrier, M. *J. Phys. Chem. Solids* **2003**, *64*, 841−846.
(36) Inokuti, M.; Hirayama, F. *J. Chem. Phys.* **1965**, *43*, 1978−1989.